

Production of fast particles in the laser plasma in experiments with the Sokol installation

V. V. Volenko, A. L. Zapysov, A. F. Ivanov, L. A. Myalitsin, L. A. Osadchuk, and
A. I. Saukov

(Submitted 5 September 1985)

Zh. Eksp. Teor. Fiz. **91**, 804–817 (September 1986)

Experiments on the interaction of laser beams with plasmas at beam power densities $q \approx 10^{13}$ – $4 \cdot 10^{14}$ W/cm² carried out at the Sokol installation are reported. The laser beams were either linearly or circularly polarized. The results can be used to draw a purely empirical physical picture of the absorption of laser energy. Detailed measurements of the properties of the fast plasma particles reveal the component of the absorption of laser energy which is due to nonclassical mechanisms. These measurements also make it possible to study the production of fast particles and, in the case of the linear polarization, to compare the experimental results with the results of the theoretical models which have been proposed. The experiments with the circular polarization, the first of their kind, reveal substantial decreases in the characteristic energies and numbers of fast ions and electrons. The results of the Sokol experiments are compared with results obtained at the Kal'mar, Del'fin, Janus, Cyclops, Argus (LLNL), and Chroma (KMS Fusion) installations.

INTRODUCTION

Experiments on the irradiation of fusion targets by intense laser beams are being carried out on a wide scale as part of the laser-fusion program both in the USSR and in foreign countries. A necessary part of laser experiments is a detailed study of the interaction of the laser beams with dense plasmas. The crucial problems are to determine the absorption coefficient for the laser energy, to identify the primary mechanism for this absorption, to measure the properties of the fast particles (electrons and ions) of the laser plasma, and to identify the mechanisms and particular features of the production of these particles under various experimental conditions. Such studies are quite urgent because of the need to formulate requirements on the parameters of the targets and of the high-power laser systems in order to obtain the conditions for achieving high densities of the DT gas, $\rho_{DT} \gtrsim 200$ g/cm³, and for achieving a fusion burn.

Studies to this end have been carried out at the Sokol 24-channel laser installation^{1,2} since it started up in 1976; these studies have now been completed. A substantial body of experimental information has been acquired. The results of the first stage of this research, in 1976–1979, showed that at a laser power density $q \approx 2 \cdot 10^{14}$ W/cm² with glass targets, using linearly polarized laser beams, the absorption coefficient is relatively low¹⁾ ($K_{ib} \approx 0.2 \pm 0.05$); that fast ions are detected in the laser plasma with energies $\epsilon_i^f \approx 100$ –200 keV; and that the continuum of the x-ray emission contains a hard component ($H\nu \gtrsim 10$ keV), due to fast electrons with a typical effective temperature $T_e^f \approx 2$ –4 keV (Refs. 3 and 4). These results have motivated a numerical simulation,³ which showed, in an approach independent of that of Ref. 5, that the steepening of the density profile^{6–8} plays an important role in the absorption of laser energy. That numerical analysis also led to an interpretation of the values of the absorption coefficient measured in experiments at the Sokol installation and promoted the construction of a calibrated

semiempirical model for the absorption which has been embodied in the ZARYA hydrodynamic numerical code.^{9,10}

In the second stage of this research, in 1980–1983, the laser energy focused on the target was essentially doubled, so that a maximum beam power density $q \approx 4 \cdot 10^{14}$ W/cm² was achieved at the target. For more detailed quantitative measurements, new diagnostic facilities were added, and experiments with circularly polarized laser light were carried out for the first time. The results obtained are important for reaching an understanding of the mechanisms for, and the particular features of, the production of fast plasma particles and for constructing a purely experimental picture of the absorption of the laser energy. It has been found that the polarization of the laser light has an important effect on the interaction with the plasma. The results of this second stage of the research are the subject of the present paper.

The experiments use gas-filled microballons, fabricated as part of this study, with an aspect ratio $R/\Delta R = 30$ –80, a shell diameter $2R \approx 110$ –140 μm , a shell thickness $\Delta R \approx 0.8$ –1.5 μm , and a DT-gas pressure $P_{DT} \approx 5$ –25 atm or with $R/\Delta R = 100$ –300, $2R \approx 140$ –180 μm , $\Delta R \approx 0.3$ –0.6 μm , and $P_{DT} \approx 1$ –10 atm. The parameters of the laser pulse are as follows: The laser energy focused on the critical target size $2R_{cr} \approx 120$ –150 μm is $E_t \approx 100$ –170 J at a pulse length (width at half-maximum) $\tau_{pls} \approx 1.0$ ns or $E_t \approx 50$ –70 J at $\tau_{pls} \approx 0.3$ ns, corresponding to the maximum beam power density at the target, $q = E_t/4\pi R_{cr}^2 \tau_{pls} \approx 4 \cdot 10^{14}$ W/cm². The energy contrast of the laser pulse is $< 10^{-6}$, while the intensity contrast is $< 10^{-10}$.

I. STUDY OF THE ABSORPTION EFFICIENCY AND ABSORPTION COEFFICIENT

The following diagnostic methods are used in these studies.

1. "Calorimetry" and "Joule": measurement of the energy E_c of the laser light which enters the target chamber,

that which strikes the target (E_t), that which is reflected by the target (E_{ref}), and that which is absorbed by the target (E_a). These measurements are carried out with closed and open calorimeters¹¹ with bulk absorption.

2. "Shock wave": measurement of the absorbed energy through detection of the propagation of a shock wave in the residual gas around the target by multiframe shadow and Schlieren photography.^{2,12}

3. "Ion": measurement of the absorbed energy and energy composition of the plasma ions by means of ion collectors.¹²

4. "Corona": study of the space-time behavior of an image of the target formed in light of the second harmonic.³

5. "x radiation": measurement of the x-ray emission continuum in the energy interval $h\nu \approx 1.5-25$ keV by means of absorbing filters.¹³

6. "Pinhole": recording of x-ray images of the target at x-ray energies $h\nu \approx 1.3, 2.6,$ and 3.5 keV with a high spatial resolution.^{14,15}

The results of the measurements show that the absorption efficiency, defined as $\varepsilon_{ib} = E_{ib}/E_c$, where E_{ib} is the absorbed energy if the energy of the fast particles of the laser plasma is ignored, has values in the range $\varepsilon_{ib} \approx 0.05-0.25$, depending on the amount of incident laser energy and on the target dimensions. The measurements of the absorption efficiency and of the interaction geometric factor f_g (the fraction of the laser energy which is incident on the target, $f_g = E_t/E_c$), reveal the absorption coefficient for laser light with a wavelength $\lambda \approx 1.06$ μm : $K_{ib} = \varepsilon_{ib}/f_g$. Figure 1 shows the absorption coefficient K_{ib} versus the power density q of the laser light which is incident on the critical region of the target: $q = E_t/4\pi\bar{R}_{cr}^2\tau_{pls}$, where \bar{R}_{cr} is the time-average radius of the region of the "corona" with the critical electron density, and τ_{pls} is the length of the laser pulse (width at half-maximum). Over the range of power densities studied, this behavior can be approximated well by $K_{ib} = K_0(q/10^{14})^{-0.5}$, where $K_0 = 0.3$.

Analysis of the results of measurements of the absorption and of the properties of the fast plasma particles shows that the primary absorption mechanism in the Sokol experiments at beam power densities in the range $q \approx 10^{13}-4 \cdot 10^{14}$ W/cm^2 is classical inverse bremsstrahlung.¹⁶

At power densities $q \gtrsim 10^{14}$ W/cm^2 resonant absorption

increases in importance,¹⁷ because³ of density profile steepening. Specifically, the measurements show that in the case of linear polarization the energy carried by the fast ions at power densities $q \approx 10^{14} - 2 \cdot 10^{14}$ W/cm^2 is $E_i^f \lesssim (0.1-0.2)E_{ib}$, and the efficiency of the resonant absorption is $\varepsilon_{ra} \lesssim 0.01$, while at $q \approx (2.0-4.0) \cdot 10^{14}$ W/cm^2 the corresponding figures are $E_i^f \approx (0.2-0.3)E_{ib}$ and $\varepsilon_{ra} \approx 0.01 - 0.02$. The energy carried by the fast electrons is $E_e^f \approx 0.03E_{ib}$ according to measurements of the hard part ($h\nu \gtrsim 10$ keV) of the x-ray emission continuum in experiments with a linear polarization (Fig. 2).

The experimental data on the absorption efficiency agree with results calculated on the efficiency of classical inverse bremsstrahlung when the refraction of the laser light in the corona and density profile steepening are allowed for. The relatively small values of ε_{ib} are due primarily to the density jump in the critical region, which is $\rho_-/\rho_{cr} \approx 0.4$ at $q \approx 1.5 \cdot 10^{14}$ W/cm^2 , according to Ref. 3. Taking these results into account, we can describe the absorption coefficient as a function of the power density by

$$K_{ib} = \frac{q_a}{q} \left(\frac{\rho_-}{\rho_{cr}} \right)^2 \frac{L}{T_e^{cr3/2}}, \quad (1)$$

where the density gradient length L in the critical region is related to the size of this region R_{cr} . According to Ref. 3, this relation is $L \approx R_{cr}/3 \propto q^{1/8}$. For spherical heat conduction in the corona, the electron temperature E_e^{cr} is related to the absorbed power density q_a by¹⁸ $T_e^{cr} \propto q_a^{2/7}$, while the jump ρ_-/ρ_{cr} can be interpolated to within $\approx 10\%$ from $\rho_-/\rho_{cr} \propto q^{-0.2}$ for power densities in the range $q \approx 10^{13}-5 \cdot 10^{14}$ W/cm^2 , according to Ref. 8. The behavior of the inverse bremsstrahlung coefficient is therefore $K_{ib} \propto q^{0.5}$, again in agreement with experiment.

Figure 1 shows a plot of the total absorption coefficient $K_a = (\varepsilon_{ib} + \varepsilon_{ra})/f_i$ versus the power density for the case of linear polarization. Also shown here are the results of measurements of the absorption coefficient in experiments at other laser installations.^{5,19-21}

II. STUDY OF THE PRODUCTION OF FAST IONS OF THE LASER PLASMA

I. According to the present physical understanding, the reason for the production of superthermal electrons and ions

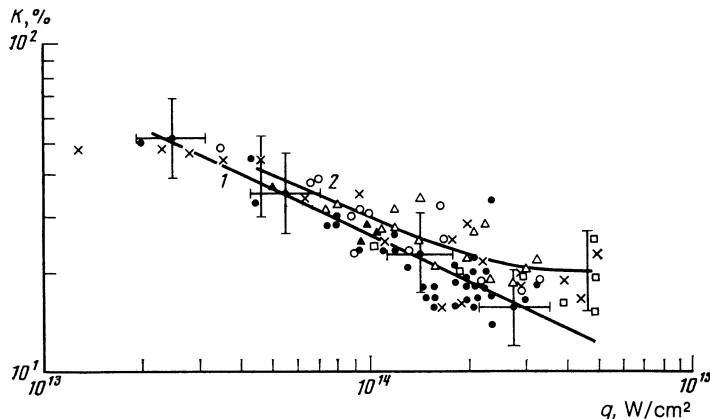


FIG. 1. Absorption coefficient versus the power density of the laser light incident on the target. ●— K_{ib} , Δ — K_a (linear polarization); ○— K_a (circular polarization, Sokol); ▲—Lebedev Physics Institute (Kal'mar, Del'fin^{19,20}); ×—LLNL (Ref. 5); □—KMS Fusion.²¹ Curve 1 is drawn through the points K_{ib} , and curve 2 through the points K_a .

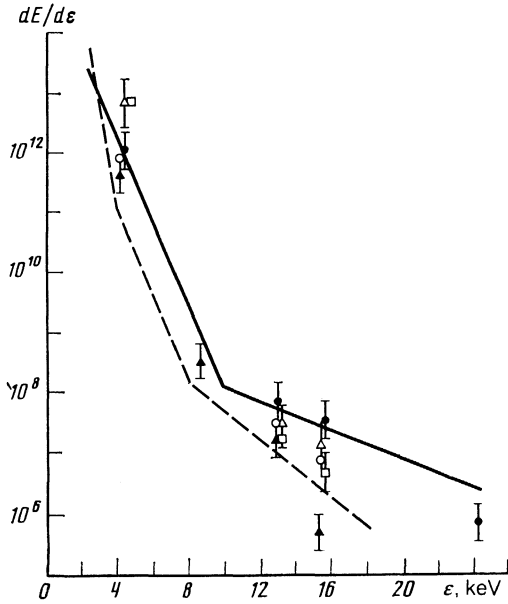


FIG. 2. The x-ray emission continuum. Linear polarization: Solid line— $q \approx 2.3 \cdot 10^{14}$ W/cm², $E_a \approx 14.5$ J (vacuum, $P_0 \approx 10^{-4}$ torr); dashed line— $q \approx 2.1 \cdot 10^{14}$ W/cm², $E_a \approx 18.8$ J (air, $P_0 \approx 3.5$ torr). Circular polarization: \blacktriangle — $q \approx 10^{14}$ W/cm², $E_a \approx 5.3$ J; \circ — $q \approx 10^{14}$ W/cm², $E_a \approx 11$ J; \square — $q \approx 2.0 \cdot 10^{14}$ W/cm², $E_a \approx 25$ J; \triangle — $q \approx 2.9 \cdot 10^{14}$ W/cm², $E_a \approx 27$ J; \bullet — $q \approx 3.8 \cdot 10^{14}$ W/cm², $E_a \approx 11$ J, $\tau_{\text{plis}} \approx 0.3$ ns.

is the strong resonant electric field which arises in the part of the corona with the critical density when p -polarized light is incident obliquely on an inhomogeneous plasma slab.¹⁷ This field accelerates electrons along the direction perpendicular to the plasma surface, to high energies

$$\langle \varepsilon_e^f \rangle = 3/2 T_e^f \approx 4 \cdot 10^{-3} (qL\lambda)^{1/2}; \quad (2)$$

here ε_e^f , and T_e^f are expressed in keV, L and λ are in centimeters, and q is in watts per square centimeter. As they are emitted from the target, the electrons create a potential which accelerates ions, by virtue of charge separation. According to an analytic model for the isothermal expansion, the ion distribution function in this case is exponential²²:

$$dN_i/dV \propto \exp(-V/V_0), \quad (3)$$

where the velocity scale V_0 is related to the temperature of the fast electrons by

$$V_0 = \frac{1}{(\nu+1)^{1/2}} \left(\frac{ZT_e^f}{Am_p} \right)^{1/2}, \quad (4)$$

where $\nu = 0, 1, 2$ for the plane, cylindrical, and spherical cases of expansion; Z and A are the atomic number and atomic weight of the ion; and m_p is the mass of the proton. Most of the fast ions have velocities $V \leq V_{\text{max}} \approx 20C_s$, where C_s is the sound velocity in the plasma. For the typical power densities at the Sokol installation, $q \approx (2.0-4.0) \cdot 10^{14}$ W/cm², the density gradient length at the jump is $L \approx 1-2 \mu\text{m}$, and the parameters $\langle \varepsilon_e^f \rangle$ and V_0 have the following values, according to (2)–(4): $\langle \varepsilon_e^f \rangle \approx 6-8$ keV and $V_0 \approx 3 \cdot 10^7$ cm/s.

In addition, we would like to discuss another mechanism, which can be outlined as follows^{23,24}: The excess pres-

sure of the resonant electric field E_* of the plasma waves causes an ejection of plasma from the region with the critical density. The maximum energy which the ions acquire in this process is determined from the relation

$$n_i Am_p V_i^2 = E_*^2 / 4\pi, \quad (5)$$

where n_i is the density of ions in the critical region. In this mechanism, the most interesting effects occur when an aperiodic instability ($t \rightarrow l + a$) sets in; this instability increases the field E_* in the resonant regions and the energy of the fast ions by a substantial amount. In this case there is a highly anisotropic distribution of fast ions, and “jets” are generated. The energy and number of the fast ions in a jet are

$$\langle \varepsilon_i^f \rangle \approx 20 Z^{1/2} A^{1/2} T_e^{1/2} (L/\lambda)^{1/2}, \quad (6)$$

$$\langle N_i^f \rangle \approx 10^8 L^{1/2} R_{\text{cr}}^2 Z^{-1} \lambda^{-1/2},$$

where λ , L , R_{cr} are all expressed in microns.

For the experimental conditions at the Sokol installation these parameters have the values $\langle \varepsilon_i^f \rangle \approx 200$ keV and $N_i^f \approx 10^{11}-10^{12}$.

2. *Linear polarization.* Production of fast ions in a laser plasma with both isotropic and highly anisotropic (“jet”) distributions has been reported in Refs. 25–30 and in experiments with Sokol. Since the detailed mechanism for the formation of jets of fast ions has not been completely investigated, and the influence of this effect on the gasdynamics of the compression has not been determined, such studies are worthwhile.

Results of optical and x-ray detection of a jet of fast ions in Sokol experiments with linearly polarized laser light were reported in Refs. 3 and 14. These results are typical of power densities $q > 10^{14}$ W/cm². The parameters of the fast ion jets were determined by the approach of Refs. 24 and 25. The ionization energy loss of the fast ions as they pass through the air is³¹ $d\varepsilon_i/dx \approx 20$ keV/cm; the specific energy Q of the cylindrical shock wave is evaluated from the scaling law^{32,33} $R_{\text{sw}} \propto (Q/\rho_0)^{1/4} t^{1/2}$. The number of fast ions in the jet is $N_i^f \propto Q(d\varepsilon_i/dx)$, and the total energy of these ions is $E_i^f \approx N_i^f \varepsilon_i^f$, where $\varepsilon_i^f = Am_p V_i^2/2$, and V_i is the velocity of the fast ions. Table I shows the results for several of the Sokol experiments. Also shown here are results found at the Kal'mar installation.^{24,25}

Because the experimental conditions at the Sokol and Kal'mar installations are similar, the properties of the fast ions are also approximately the same. The energy carried off by the fast ions in the jet is $\approx 5-10\%$ of the absorbed energy E_{ib} . The jets of fast ions in these experiments were observed only at power densities $q \gtrsim 10^{14}$ W/cm². At power densities $q \approx (1.0-2.0) \cdot 10^{14}$ W/cm² at the target, jets were not generated in all experiments, while for $q \gtrsim 2 \cdot 10^{14}$ W/cm² jets were generated in each experiment, in a number of three to five, implying an increase in the role of the resonant interaction. The total energy of the fast ions in the jets at $q \approx (2.0-4.10) \cdot 10^{14}$ W/cm² is related to the absorbed energy by $E_i^f \approx (0.2-0.3) E_{\text{ib}}$.

The jets of fast ions observed in the Sokol experiments are emitted from the target in approximately the same direc-

TABLE I.

	$q, \text{W/cm}^2$	$Q, \text{J/cm}$	N_i^f	N_{SiO_2}	N_i^f/N_{SiO_2}	ϵ_i^f, keV	E_i^f, J	F_{ib}, J
Sokol	$1.2 \cdot 10^{14}$	0.1	$4 \cdot 10^{13}$	$3 \cdot 10^{15}$	0.01	100	0.7	8
	$1.9 \cdot 10^{14}$	0.2	$8 \cdot 10^{13}$	$3.6 \cdot 10^{15}$	0.02	100	1.5	11.7
	$2.1 \cdot 10^{14}$	0.1	$3 \cdot 10^{13}$	$2.5 \cdot 10^{15}$	0.01	300	1.5	18.8
Kal'mar	10^{14}	0.05	$2 \cdot 10^{13}$	$2 \cdot 10^{15}$	0.01	500	1.5	7.5-15

Q is the specific energy of the cylindrical shock wave, and N_{SiO_2} is the number of SiO_2 molecules in the target.

tions in different experiments. The jet directions were not found to be isotropic, so that it was possible to position ion collectors along the most probable jet directions and to measure the ion velocity distributions $f_i(V)$ in experiments under high-vacuum conditions ($P_0 \approx 10^{-4} - 10^{-5}$ torr) in the target chamber:

$$f_i(V) = i(t) r_c / \bar{Z}_{\text{eff}} e \Omega V^2, \quad (7)$$

where $i(t)$ is the total current drawn by the collector, $\bar{Z}_{\text{eff}} e$ is the average charge formed at the collector as the result of the interaction with the plasma ion, Ω is the solid angle of the

collector, and r_c is the distance from the target to the collector. Figure 3 shows the ion currents and the velocity distributions measured in experiments with a linear polarization at power densities $q \approx (0.3 - 3.0) \cdot 10^{14} \text{ W/cm}^2$. Curves 2 correspond to the case in which a collector is oriented in the direction in which the jets of fast ions are produced; curves 1 correspond to the thermal distribution of the ions of the laser plasma. These results show that at a power density $q \approx 3.0 \cdot 10^{13} \text{ W/cm}^2$ no fast ions are produced; the two distribution functions are approximately the same and are thermal. With increasing power density, a peak corresponding to fast ions with $V_i \approx 10^8 \text{ cm/s}$ appears on the ion current drawn by collectors 2 at $t \approx 100 - 200 \text{ ns}$, and in the high-energy region the ion distribution function (2) is about an order of magnitude above a thermal distribution.

Table II shows the typical velocities of the fast ions, V_0 , and the corresponding energies ϵ_i^f . Also shown here are the temperatures T_e^f measured for the fast electrons from the x-ray continuum spectra at high energies $\bar{h\nu} \gtrsim 10 \text{ keV}$ and calculated from the measured values of V_0 in accordance with (4) for spherical expansion. The typical velocities V_0 are $V_0 \approx (1.0 - 1.5) \cdot 10^8 \text{ cm/s}$; these figures correspond to energies $\epsilon_i^f \approx 100 - 250 \text{ keV}$ of the fast ions in a jet. The temperature of the fast ions calculated from (4) is $T_e^f \approx 50 - 150 \text{ keV}$, $\approx 10 - 30$ times the values measured in these experiments, $T_e^f \approx 2 - 4 \text{ keV}$. This result means that the fast electrons with average energies $\langle \epsilon_e^f \rangle \approx 3 - 6 \text{ keV}$ produced in these experiments cannot, as they fly away from the target, create electrostatic potentials which accelerate ions to energies $\epsilon_i^f \approx 100 - 250 \text{ keV}$.

The high-energy part of the x-ray continuum was reliably detected in experiments with the linear polarization at the Sokol installation at power densities $q > 1.0 \cdot 10^{14} \text{ W/cm}^2$ at the target. At power densities $q < 10^{14} \text{ W/cm}^2$, the hard component of the x-ray spectrum was not detected; the corresponding intensities at $h\nu > 10 \text{ keV}$ were below the detection threshold $dE/d(h\nu) \approx 5 \cdot 10^5$. This result corresponds to a decrease in the number of fast electrons by a substantial factor, more than $\sim 10^2$. The jets of fast ions, in contrast, were detected experimentally even in the absence of the hard component of the spectrum at power densities $q \sim 10^{14} \text{ W/cm}^2$ and had the same parameter values as in Table I.

These aspects of the production of the jet of fast ions and the parameter values of these jets imply a ponderomotive mechanism for the plasma acceleration^{23,24} and are evidence in favor of this mechanism. According to Ref. 24, a power density $q \approx 10^{14} \text{ W/cm}^2$ is sufficient for the onset of an

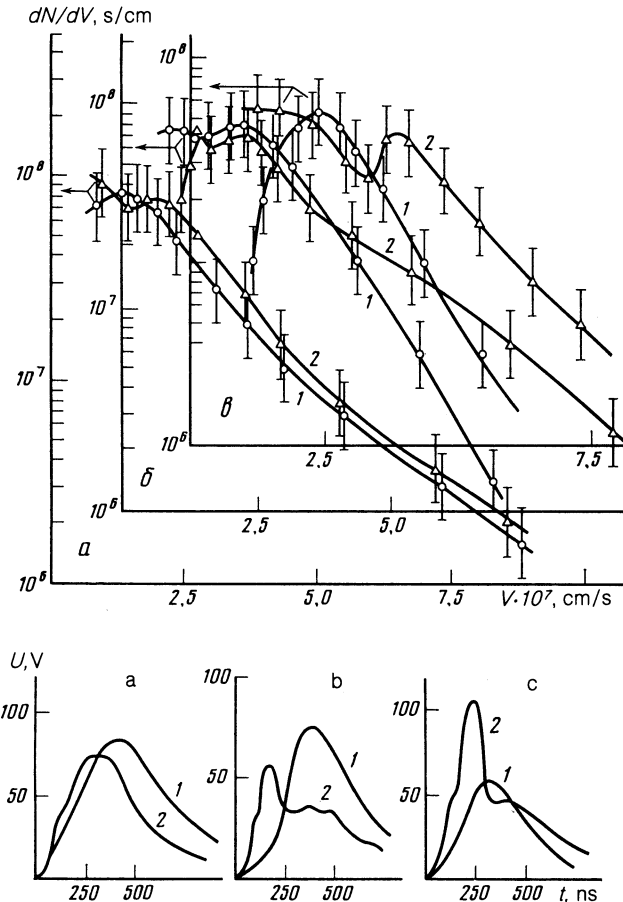


FIG. 3. Temporal shape of the signal from the ion collector $U(t)$; ion velocity distribution function dN/dV . a: $q \approx 3.0 \cdot 10^{13} \text{ W/cm}^2$. b: 10^{14} W/cm^2 . c: $1.5 \cdot 10^{14} \text{ W/cm}^2$. Δ, \circ —experimental points. The errors in the measurement of the absolute values of the distribution function, including the error in the calibration of the collectors, is shown in Figs. 3 and 5. The error in the determination of the dependence of the distribution function on the ion velocity in relative units, is substantially smaller, $\approx 10\%$.

TABLE II.

Experiment	q , W/cm ²	$V_0 \cdot 10^7$ cm/s	ϵ'_i , keV	T'_e , keV	T'_e , keV, calc. from (4)
47	$3 \cdot 10^{13}$	7.3	56	—	34
48	$3 \cdot 10^{14}$	15	234	2.5	140
49	$2 \cdot 10^{14}$	11	126	—	76
50	10^{14}	13	176	2.0	106
51	$1.5 \cdot 10^{14}$	8.5	75	2.0	45
52	$2.3 \cdot 10^{14}$	9.9	88	3.6	53
53	$1.4 \cdot 10^{14}$	14	192	4.2	115
55	$1.7 \cdot 10^{14}$	11	126	3.1	76

aperiodic parametric instability, since the threshold for this instability is

$$q_n^{i \rightarrow i+a} \approx 10^{13} e^{\tau} \lambda^{-3} T_e^{-1/2} (\bar{Z} + 2.5 T_e^2 \lambda^2 / L) \approx 10^{14} \text{ W/cm}^2, \quad (8)$$

where τ is the optical thickness of the plasma.

Further confirmation of this interpretation comes from the fact that jets are detected in the integrated x-ray images at x-ray energies $\hbar\nu + 1.3$ keV. In the case of the ponderomotive mechanism, the plasma as a whole is ejected from the critical region, and its nonequilibrium thermal emission is detected in the x-ray images. The image of a jet cannot result from bremsstrahlung of the fast electrons as they pass through the plasma, since the intensity of the hard component in the x-ray spectrum, at ~ 1 – 2 keV, is ≈ 3 – 4 orders of magnitude below the intensity of the x-ray emission from the corona (Fig. 2). In the x-ray images measured, on the other hand, the densities of the blackening in the corona and in the jet are approximately the same.

We note in conclusion that the source of perturbations for the onset of a parametric instability may be fluctuations of the intensity of the laser light. These fluctuations may in turn be intensified by self-focusing^{27,34} in the plasma corona of initial coherent bursts in the distribution³⁵ of the power density of the incident light on the target surface. On the other hand, the reproducibility of the spatial orientation of the fast-ion jets arises because the conditions obtain for the onset of the aperiodic parameter interaction process in some part of the corona because the polarizational, angular, and

fluctuational composition of the laser light in this region is the optimum for the given instability. Confirmation of this interpretation comes from the experimental fact (established by the present authors) that the directions of the jets change when the structure of the optical system which focuses the laser light on the target is changed. This change was carried out between different series of experiments (with 25–30 experiments per series). The features of the jets reported here correspond, in the terminology of Refs. 36–38, to the properties of spicules: narrow jets of plasma with a density well above the density of the surrounding expanding plasma.³⁹

3. Circular polarization. The results obtained in this case are quite different from the results of the experiments with the linear polarization. Figure 4 shows x-ray images characterizing experiments with a circular polarization. The perturbations of the plasma corona which are detected are generally not the narrow, needle-shaped jets found in the earlier series of experiments at power densities $q \gtrsim 10^{14}$ W/cm²; instead, they are more diffuse and more suggestive of the nonuniformity of the plasma expansion. A significant series (of about 40) experiments with circular polarization showed that the nature of the perturbations of the corona which were detected changes from an essentially uniform distribution of jets over the sphere to cases of the production of single jets or the complete absence of jets. We did not find any regular behavior in the results of the measurements of the x-ray images. We can only point out that the jets were

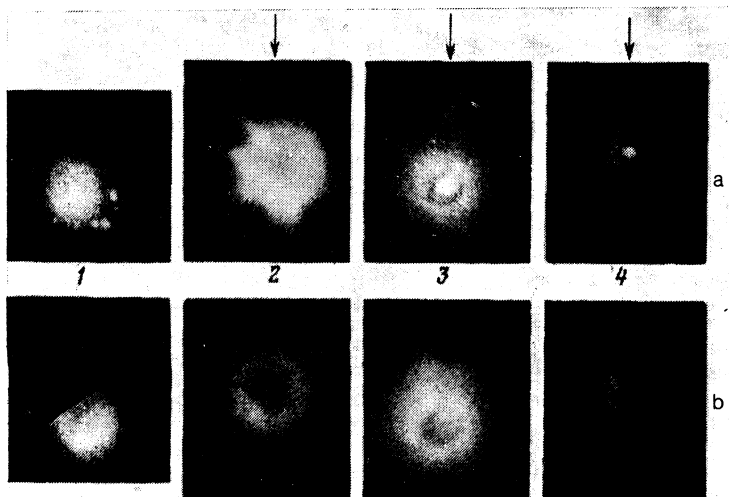


FIG. 4. Time-integrated x-ray images of the target in experiments with circular polarization and x-ray energies (a) $\hbar\nu \approx 1.3$ keV and (b) 2.6 keV. 1— $q \approx 10^{14}$ W/cm²; 2— $1.2 \cdot 10^{14}$ W/cm²; 3— $2.9 \cdot 10^{14}$ W/cm²; 4— $3.5 \cdot 10^{14}$ W/cm². The arrows show the target suspension.

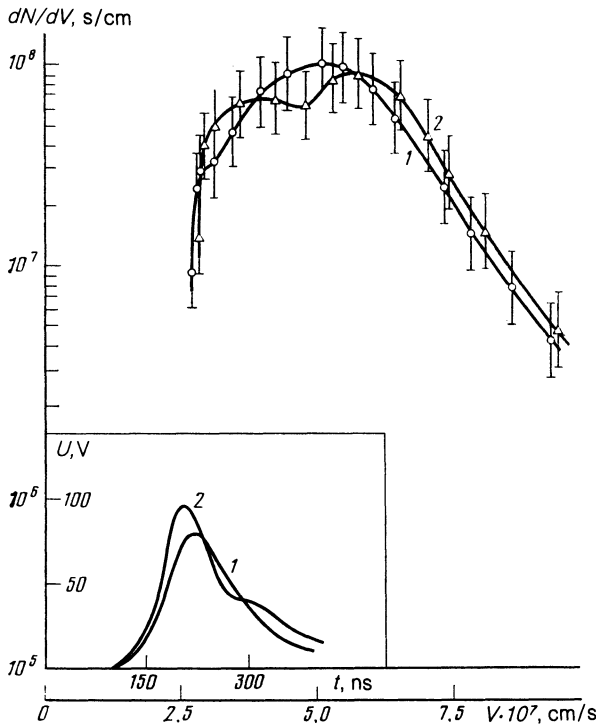


FIG. 5. Temporal shape of the signal from the ion collector, $U(t)$, and ion velocity distribution function dN/dV in experiments with circular polarization. Here $q \approx 10^{14}$ W/cm² (the notation is the same as in Fig. 3).

never observed on x-ray images with $\bar{h\nu} \approx 2.6$ keV, in the case of either linear or circular polarization.

Figure 2 shows the results found in measurements of the x-ray emission continuum in experiments with a circular polarization. Comparison with the typical x-ray spectrum measured in the case of the linear polarization shows that the intensity in the soft part of the spectrum (the point $\bar{h\nu} \approx 4.0$ keV) remains essentially the same for experiments with roughly the same amount of absorbed energy, and it increases severalfold in experiments in which the absorbed energy increases by a factor of 1.5–2. The intensity in the hard part of the x-ray spectrum (the points $\bar{h\nu} \approx 13.2$ and 15.6 keV), on the other hand, in the experiments with the circular polarization and with approximately equal power densities on the target is several times lower, even at an absorbed energy higher by a factor ≈ 2 . The intensity of the x-ray emission at x-ray energies $\bar{h\nu} \approx 24.3$ keV at power densities $q < 3 \cdot 10^{14}$ W/cm² is always below the detection threshold $dE/d(h\nu) < 5 \cdot 10^5$. The only exceptional case was experiment No. 57, where a maximum power density $q \approx 3.8 \cdot 10^{14}$ W/cm² was reached at a laser pulse length $\tau_{\text{pls}} \approx 0.3$ ns, and an x-ray emission intensity $dE/d(h\nu) \approx 5.7 \cdot 10^5$ was measured at the point $\bar{h\nu} \approx 24.3$ keV. This result is evidence that the effective temperature of the fast electrons and the number of these electrons decreases by a factor of several times unity in experiments with circular polarization compared with the values in the case of linear polarization, for given values of the power density and the absorbed energy.

Figure 5 shows the results of a study of the ion velocity

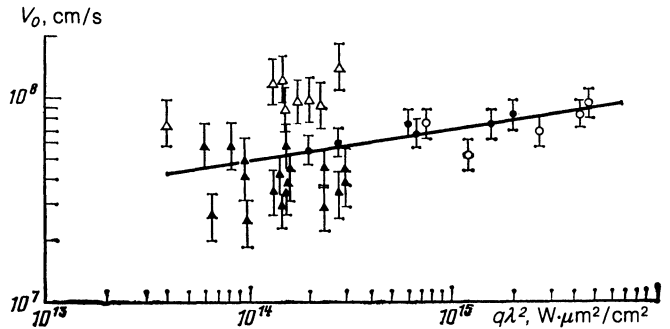


FIG. 6. Typical energy of the fast ions, V_0 , versus the reduced value of the power density, $q\lambda^2$. Δ —Sokol, linear polarization ($\lambda = 1.06$ μm); \blacktriangle —Sokol, circular polarization ($\lambda \approx 1.06$ μm); \circ —Chroma ($\lambda \approx 1.05$ μm); \bullet —Chroma, linear polarization ($\lambda \approx 0.53$ μm) (Ref. 20). The solid line is a least-squares approximation of the data of Ref. 29 and corresponds to a behavior $V_0 \propto (q\lambda^2)^{0.3}$.

distribution; these results are typical of the experiments with the circular polarization. In this case, no substantial differences were observed in the results detected by ion collectors in different directions. The ion distribution functions are similar to each other both for the different collectors in a given experiment and for different experiments, regardless of the nature of the x-ray images detected. This result is evidence of a much more nearly isotropic energy distribution of the ions of the laser plasma. The ion distribution functions show fast ions with typical velocities smaller by a factor ≈ 2 –4, i.e., $V_0 \approx (2\text{--}3) \cdot 10^7$ cm/s, in a number about an order of magnitude smaller than in the case of the linear polarization. A maximum ion velocity $V_m \approx 10^8$ cm/s was detected on the distribution function; this velocity corresponds to $V_m \approx 16C_s$. These results are evidence of a significant decrease in the typical velocities of the fast ions and in the number of these ions in the case of the circular polarization for given values of the laser power density at the target.

The particular features of the jets found in the experiments with the circularly polarized laser light are approximately the same as the properties of the jets. The mechanism for the generation of these jets is presently being studied experimentally and theoretically.^{36–39}

Figure 6 shows the typical velocity V_0 as a function of the reduced power density $q\lambda^2$ for the cases of linear and circular polarization of the light. Also shown here are results of measurements of the parameters of the fast ions in experiments with laser wavelengths $\lambda \approx 1.05$ and 0.53 μm at the Chroma installation.²⁹ Figure 1 shows the absorption coefficient versus the power density for the case of the circular polarization.

4. The collector measurements show that the mass of the fast ions carried out in a jet into the solid angle of the ion probe is, e.g., for the experiment in Fig. 3, $m_i^f \approx 1.2 \cdot 10^{-12}$ g, while the mass of all the thermal ions carried out in the solid angle of this probe is $m_i^{\text{th}} \approx 1.2 \cdot 10^{-11}$ g, for the given experiment. Since the velocity of the fast ions is more than an order of magnitude higher than the velocity of the thermal ions, $V_i^f \approx (1.0\text{--}2.0) \cdot 10^8$ cm/s versus $V_i^{\text{th}} \approx (1.0\text{--}2.0) \cdot 10^7$ cm/s, the momentum carried off by the fast ions is comparable to

the momentum carried off by the thermal component of the laser plasma into the given solid angle. This result is evidence that the production of fast-ion jets leads to perturbations of the spherical symmetry of the plasma expansion and of the ablation pressure at the part of the shell which has not evaporated.

The result shown in Fig. 4 indicate a relationship between the perturbations of the symmetry found in the x-ray images and the production of a jet in a specific part of the target. In the parts of the target where the jets are generated, dips in the emission intensity over the entire width of the outer ring, formed by nonequilibrium radiation from the heat-conduction region, are detected on the x-ray images with an x-ray energy $h\nu \approx 2.6$ keV. The radius of the inner boundary of the outer ring, which is approximately equal to the radius of the evaporation front at the time of the target collapse, according to gasdynamic calculations by the ZARYA code,^{9,10} has a large value in the jet production region. This result is evidence that at the time of the collapse the evaporation front in this region is far from the center of the target. This circumstance reduces the degree of compression of the DT gas.

In no experiment was destruction of the shell due to the production of fast-ion jets detected before the time at which the shell collapsed. The central maximum on the x-ray images, due to the radiation from the compressed part of the target, is reliably detected even when jets are produced. Analysis and comparison with the results of gasdynamic calculations show that the dimensions of this central maximum are essentially the same as the calculated values and imply a high degree of compression of the part of the target which has not evaporated. However, the fact that the neutron yield is much lower (by a factor $\sim 10^3$ – 10^5) than predicted by the gasdynamic calculations^{14,15} (a neutron yield at the level $\sim 10^3$ was detected in only a few experiments; the threshold of the neutron method is $\approx 5 \cdot 10^2$) implies that the tempera-

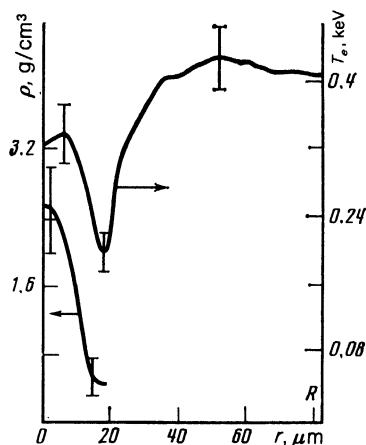


FIG. 7. Reconstructed radial profiles of the plasma electron temperature T_e and the density of matter, ρ , in the compressed part of the target. Experiment with $2R \approx 170.8 \mu\text{m}$, $\Delta R \approx 0.47 \mu\text{m}$, $R/\Delta R \approx 182$, $P_{\text{DT}} \approx 10$ atm, $q \approx 2.9 \cdot 10^{14} \text{ W/cm}^2$, $\tau_{\text{plis}} \approx 1.0$ ps, $E_a \approx 26.7$ J. The error in the reconstruction of the radial profiles in relative units is shown in this figure. The errors in the determination of the absolute values of the temperature and density, on the other hand are $\Delta T_e/T_e \approx 20\%$ and $\Delta\rho/\rho \approx 70\%$.

ture of the DT gas and its density are significantly reduced (by a factor ≈ 3 – 5). A numerical analysis of the x-ray images which reconstruct the radial profiles of the electron temperature of the plasma and of the density of the medium in the compressed part of the target indicates complete mixing of the DT gas and the glass in the compressed region (Fig. 7). The primary reason for this circumstance is the onset of a Rayleigh-Taylor hydrodynamic instability at the boundary where the DT gas makes contact with the glass and thus the turbulent mixing of the gas and the glass in the stage of the deceleration of the shell.^{40,41} Consequently, the perturbations introduced by the jets, which are also short-wave perturbations, with $\Delta l \approx 2R_{\text{cr}} (V_i^{\text{th}}/V_i^f) \approx 10 \mu\text{m}$ [the index of the harmonic is $n = 2\pi R_{\text{cr}}/\Delta l \approx \pi (V_i^f/V_i^{\text{th}}) \approx 30$], can also be included among the sources of the short-wave perturbations of the spherical symmetry which are accentuated as a result of the onset of the hydrodynamic instability (in addition to the “roughness” of the surfaces of the shell and the short-wave component of the nonuniformity of the illumination of the target³⁵).

Since the fast ions of the laser plasma are produced not in the evaporation region but in the region of the critical density, the magnitude of the reaction momentum transferred to the part of the shell which has not evaporated is generally different from the momentum of the fast ions. The importance of a detailed study of the effect of the generation of the jet of fast ions on the stability of the compression of spherical targets for the laser-fusion problem, on the other hand, in connection with the stiff requirements on the symmetry of the targets and the uniformity of their illumination,³⁵ requires gasdynamic calculations by two-dimensional codes in addition to experiments in laser installations.

5. Figure 2 also shows the x-ray emission continuum measured in experiments on Sokol with residual air in the target chamber: $P_0 \approx 3.5$ torr, $\rho_0 \approx 6 \cdot 10^{-6} \text{ g/cm}^3$. The power density of the laser light at the target and the absorbed energy in these experiments were approximately the same as in experiments carried out in high vacuum ($P_0 < 10^{-4}$ torr): $q \approx (2\text{--}2.5) 10^{14} \text{ W/cm}^2$ and $E_a \approx 15\text{--}20$ J, respectively. These results show that at x-ray energies $h\nu > 3$ keV the spectral intensity of the emission in the experiments carried out in the air is about an order of magnitude lower than the intensity in the experiments in vacuum. The reason for this difference is the presence of the gas in the target chamber.⁴ As the high-energy electrons of the laser plasma (which determined the x-ray emission of the plasma at $h\nu > 3$ keV enter the region of cool plasma and heated residual gas around the target, they do not return to the region of the hot corona. The electric charge which they carry off is neutralized by a countercurrent of electrons from the heated gas. According to Refs. 42 and 43, electrons with energies $\varepsilon_e < T_e^{\text{cr}} \ln(\rho_{\text{cr}}/\rho_0) \approx 6.5 T_e^{\text{cr}} \approx 3\text{--}4$ keV return to the region of dense plasma. This result agrees with the measurements. On the other hand, at an air pressure $P_0 < 10^{-4}$ torr there is no compensation for the loss of charge from the corona, and the high-energy electrons return to the region of dense plasma.

The recombination of high-energy electrons with multiple charged ions of the laser plasma, which dominates the x-

ray emission at energies $h\nu > 3$ keV, is therefore suppressed in the experiments in air by the escape of these electrons from the hot part of the corona. This process is extremely important for controlling the experiments carried out in the laser-fusion program.

CONCLUSION

In the experiments carried out at the Sokol installation, studies have been made of the efficiency of the absorption of laser energy, the coefficient of this absorption, the properties of the fast plasma particles, and the particular features of the production of these particles over a broad range of power densities, $q \approx 10^{13} - 4 \cdot 10^{14}$ W/cm², for linearly and circularly polarized laser light.

Analysis of the results of measurement of the absorption efficiency and of the properties of the fast ions and electrons of the laser plasma shows that the primary mechanism for the absorption over the range of power densities studied is the classical mechanism of inverse bremsstrahlung. At power densities $q \gtrsim 10^{14}$ W/cm², resonant absorption increases in importance because the density profile steepens.

The particular features of the production of the fast-ion jets and the properties of these jets which have been studied in the case of linearly polarized laser light correspond to a ponderomotive mechanism for the acceleration of the plasma. It has been found that the production of jets affects the gasdynamics of the compression of laser targets.

Detailed measurements of the properties of the fast plasma particles in experiments with circularly polarized laser light, carried out on Sokol for the first time, show that there is a substantial decrease in the characteristic energies of the fast ions and electrons and in the number of these particles. The results found in these experiments are very important for establishing the experimental conditions required for achieving high densities of the thermonuclear fuel in low-entropy laser targets. Furthermore, these results are clearly of interest for deriving a theory for the nonclassical interaction of intense, circularly polarized laser light with a dense plasma, which is not presently available.

¹¹The total values of the absorbed energy, of the absorption efficiency, and of the absorption coefficient are denoted as E_a , ϵ_a , and K_a here. The contributions of the individual absorption mechanisms are instead denoted as E_{ib} , ϵ_{ib} , and K_{ib} (the classical inverse bremsstrahlung) or E_{ra} , and ϵ_{ra} (resonant absorption).

¹V. V. Volenko, A. I. Zuev, and A. F. Ivanov *et al.*, Trudy III Vsesoyuznoi konferentsii "Optika lazerov" (Proceedings of the Third All-Union Conference on Laser Optics), Leningrad, 4-8 January 1982, p. 12.

²I. A. Abramov, V. V. Volenko, and N. P. Voloshin *et al.*, Zh. Eksp. Teor. Fiz. **83**, 988 (1982) [Sov. Phys. JETP **56**, 557 (1982)].

³Yu. A. Zysin, I. A. Abramov, and V. V. Volenko *et al.*, Zh. Eksp. Teor. Fiz. **83**, 1346 (1982) [Sov. Phys. JETP **56**, 773 (1982)].

⁴A. S. Ganeev, A. L. Zapysov and A. I. Zuev *et al.*, Kvant. Elektron. (Moscow) **9**, 711 (1982) [Sov. J. Quantum Electron. **12**, 439 (1982)].

⁵H. D. Shay, R. A. Haas, and W. L. Kruer *et al.*, Phys. Fluids **21**, 1634 (1978).

⁶K. A. Brueckner and R. S. Janda, Nucl. Fusion **17**, 451 (1977).

⁷D. T. Attwood, D. W. Sweeney, J. M. Auerbach, and P. H. Y. Lee, Phys. Rev. Lett. **40**, 184 (1978).

⁸A. Raven and O. Willi, Phys. Rev. Lett. **43**, 278 (1979).

⁹A. I. Zuev, N. G. Karlykhanov, V. A. Lykov, and V. E. Chernyakov,

Preprint No. 37, Inst. Appl. Math., Academy of Sciences of the USSR, 1980.

¹⁰E. N. Avrorin, A. I. Zuev, N. G. Karlykhanov, V. A. Lykov, and V. E. Chernyakov, Preprint No. 48, Inst. Appl. Math., Academy of Sciences of the USSR, 1980.

¹¹B. L. Vasin, N. N. Zorev, and V. N. Radaev *et al.*, Prib. Tekh. Eksp. No. 2, 176 (1980).

¹²V. V. Volenko, A. L. Zapysov, and A. I. Zuev *et al.*, Kvant. Elektron. (Moscow) **11**, 44 (1984) [Sov. J. Quantum Electron. **14**, 26 (1984)].

¹³A. S. Ganeev, A. L. Zapysov, and I. M. Izrailev *et al.*, Kvant. Elektron. (Moscow) **7**, 2227 (1980) [Sov. J. Quantum Electron. **10**, 1294 (1980)].

¹⁴V. V. Volenko, A. I. Zuev, and A. F. Ivanov *et al.*, Kvant. Elektron. (Moscow) **10**, 2350 (1983) [Sov. J. Quantum Electron. **13**, 1529 (1983)].

¹⁵V. V. Volenko, A. F. Ivanov, and L. A. Myalitsin *et al.*, Pis'ma Zh. Eksp. Teor. Fiz. **37**, 328 (1983) [JETP Lett. **37**, 389 (1983)].

¹⁶L. Spitzer, Physics of Fully Ionized Gases, Interscience, New York, 1956 (Russ. transl., IIL, Moscow, 1957).

¹⁷Yu. V. Afanas'ev, N. G. Basov, and O. N. Krokhin *et al.*, Vzaimodeistvie moshchnogo lazernogo izlucheniya s plamoĭ. Itogi nauki i tekhniki (Interaction of Intense Laser Radiation with Plasmas, Scientific and Technological Progress), Viniti, Vol. 47, 1978.

¹⁸E. N. Avrorin, Fiz. Plazmy **7**, 694 (1981) [Sov. J. Plasma Phys. **7**, 381 (1981)].

¹⁹Yu. V. Afanas'ev, N. G. Basov, and B. L. Vasin *et al.*, Zh. Eksp. Teor. Fiz. **77**, 2539 (1979) [Sov. Phys. JETP **50**, 1229 (1979)].

²⁰N. G. Basov, A. E. Danilov, and B. V. Kruglov *et al.*, Kvant. Elektron. (Moscow) **9**, 395 (1982) [Sov. J. Quantum Electron. **12**, 225 (1982)].

²¹D. C. Slater, G. E. Busch, and G. Charatis *et al.*, Phys. Rev. Lett. **46**, 1199 (1981).

²²P. Church, R. Martin, and H. Pepin, J. Appl. Phys. **53**, 1982 (1982).

²³V. P. Silin, Zh. Eksp. Teor. Fiz. **21**, 333 (1975) [*sic*].

²⁴N. E. Andrev, Yu. A. Zakharenkov, N. N. Zorev, V. T. Tikhonchuk, and A. S. Shikanov, Zh. Eksp. Teor. Fiz. **76**, 976 (1979) [Sov. Phys. JETP **49**, 492 (1979)].

²⁵Yu. A. Zakharenkov, O. N. Krokhin, G. V. Sklizkov, and A. S. Shikanov, Pis'ma Zh. Eksp. Teor. Fiz. **25**, 415 (1977) [JETP Lett. **25**, 388 (1977)].

²⁶H. Azechi, Y. Sakagami, T. Yamanaka, and C. Yamanaka, Appl. Phys. Lett. **30**, 187 (1977).

²⁷I. V. Aleksandrova, N. G. Basov, and A. A. Galichĭ *et al.*, Pis'ma Zh. Eksp. Teor. Fiz. **38**, 60 (1983) [JETP Lett. **38**, 68 (1983)].

²⁸P. M. Campbell, R. R. Johnson, F. J. Mayer, L. V. Powers, and D. C. Slater, Phys. Rev. Lett. **39**, 274 (1977).

²⁹"Inertial Fusion Research Annual Technical Report," KMS Fusion KMSF-V1110, 1982, p. 2.

³⁰J. H. Tan, G. H. McCall, A. H. Williams, Phys. Fluids **27**, 296 (1984).

³¹I. K. Kikoin (editor), Tablitsy fizicheskikh velichin (Tables of Physical Quantities), Atomizdat, Moscow, 1976, p. 953.

³²L. I. Sedov, Metody podobiya i razmernosti mekhaniki, Nauka, Moscow, 1965 (Similarity and Dimensionality Methods in Mechanics, Academic, New York, 1959).

³³Ya. B. Zel'dovich and Yu. P. Raĭzer, Fizika udarnykh voln i vysokotemperaturnykh gidrodinamicheskikh yavlenĭi, Nauka, Moscow, 1966 [Physics of Shock Waves and High-Temperature Hydrodynamic Phenomena, Academic, New York, 1966].

³⁴C. E. Max, Phys. Fluids **19**, 74 (1976).

³⁵V. V. Volenko and V. B. Kryutsenkov, Kvant. Elektron. (Moscow) **6**, 1343 (1979) [Sov. J. Quantum Electron. **9**, 789 (1979)].

³⁶Rutherford Appleton Laboratory Annual Report, RL-82-039, 1982.

³⁷M. J. Herbst, R. R. Whitlock, and F. C. Young, Phys. Rev. Lett. **47**, 91 (1981).

³⁸M. J. Herbst, R. R. Whitlock, P. H. Lemberg, J. A. Stamper, and B. H. Ripin, Phys. Rev. Lett. **40**, 328 (1981).

³⁹I. Limpouk and V. B. Rozanov, Kvant. Elektron. (Moscow) **11**, 1416 (1984) [Sov. J. Quantum Electron. **14**, 955 (1984)].

⁴⁰V. E. Neuvazhaev Dokl. Akad. Nauk SSSR **222**, 1053 (1975) [Sov. Phys. Dokl. **40**, 398 (1975)].

⁴¹V. A. Lykov, V. A. Murashkina, V. E. Neuvazhaev, L. P. Shibarshov, and V. G. Yakovlev, Dokl. Akad. Nauk SSSR **30**, 339 (1979) [Sov. Phys. Dokl. **30**, 314 (1979)].

⁴²B. Yaakobi, J. Pelah, and H. Hoose, Phys. Rev. Lett. **37**, 836 (1976).

⁴³R. F. Benjamin, G. H. McCall, and A. W. Ehler, Phys. Rev. Lett. **42**, 890 (1979).

Translated by Dave Parsons